

See discussions, stats, and author profiles for this publication at: <https://www.researchgate.net/publication/231341583>


# Interpretation of the Temperature Dependence of the EPR Spectrum of Cu2+-Doped (NH4)2[Cd(NH3)2(CrO4)2] and Crystal Structures of the High- and Low-Temperature Forms of the Host Lat...

ARTICLE IN INORGANIC CHEMISTRY · OCTOBER 1995  
Impact Factor: 4.76 · DOI: 10.1021/cr95126a023

CITATIONS  
16


READS  
15

12 AUTHORS, INCLUDING:



**Horst Stratemeier**  
University of Tasmania  
60 PUBLICATIONS 944 CITATIONS

SEE PROFILE



**Paul T. Beurskens**  
Radboud University Nijmegen  
255 PUBLICATIONS 2,307 CITATIONS

SEE PROFILE

# Interpretation of the Temperature Dependence of the EPR Spectrum of $\text{Cu}^{2+}$ -Doped $(\text{NH}_4)_2[\text{Cd}(\text{NH}_3)_2(\text{CrO}_4)_2]$ and Crystal Structures of the High- and Low-Temperature Forms of the Host Lattice

Henrietta Headlam, Michael A. Hitchman,\* and Horst Stratemeier

Chemistry Department, University of Tasmania, Box 252C, Hobart, Tas 7001, Australia

Jan M. M. Smits,<sup>†</sup> Paul T. Beurskens,<sup>†</sup> Engbert de Boer,<sup>†</sup> and Gerrit Janssen<sup>‡</sup>

Crystallography Laboratory and Department of Molecular Spectroscopy, University of Nijmegen, Toernooiveld, 6525 ED Nijmegen, The Netherlands

Bryan M. Gatehouse, Glen B. Deacon, and Greg N. Ward

Chemistry Department, Monash University, Clayton, VIC 3168, Australia

Mark J. Riley

Chemistry Department, Queensland University, Brisbane, Queensland 4072, Australia

Deming Wang

Centre for Magnetic Resonance, Queensland University, Brisbane, Queensland 4072, Australia

Received February 9, 1995<sup>⊗</sup>

The crystal structure of  $(\text{NH}_4)_2[\text{Cd}(\text{NH}_3)_2(\text{CrO}_4)_2]$  is reported. Below about 300 K the compound changes from a monoclinic cell (space group  $C2/m$ ,  $Z = 2$ ,  $a = 12.8380(11)$  Å,  $b = 6.0308(6)$  Å,  $c = 7.5890(6)$  Å,  $\beta = 110.154(14)^\circ$ ) in which all four Cd–O bonds of the *trans*- $\text{Cd}(\text{NH}_3)_2\text{O}_4$  coordination sphere are crystallographically equivalent to a triclinic cell (space group  $P\bar{1}$ ,  $Z = 1$ ,  $a = 6.0210(4)$  Å,  $b = 7.0363(4)$  Å,  $c = 7.5714(8)$  Å,  $\alpha = 106.802(18)$ ;  $\beta = 93.032(12)$ ;  $\gamma = 114.079(11)^\circ$ ) in which the only symmetry element of the Cd complex is an inversion center. It is shown that the previously reported temperature dependence of the EPR spectrum of  $\sim 0.3\%$   $\text{Cu}^{2+}$  doped into this compound is consistent with the change in crystal structure. The spectra may be explained using a model of dynamic vibronic coupling in which the effects of Jahn–Teller coupling and a “strain” due to the inequivalence of the ligands are applied to the  $e_g$  vibrational and  $E_g$  electronic wave functions of the  $\text{Cu}^{2+}$  ion. The balance between the ligand field asymmetry and the natural tendency of  $\text{Cu}^{2+}$  to adopt a tetragonally elongated octahedral coordination geometry results in a complex with an orthorhombic coordination geometry having short bonds to the ammine groups and intermediate and long bonds to the chromate oxygen atoms. However, the long Cu–O bonds may occur to either pair of *trans* chromate oxygen atoms. In the high-temperature monoclinic unit cell, the EPR spectrum confirms that these two conformations are energetically equivalent, but in the low-temperature triclinic cell this is no longer the case, and the EPR spectrum is consistent with a temperature-dependent equilibrium between the two possible structural isomers. However, the model suggests that significant delocalization of the vibronic wave functions may occur, so that it is difficult to define precisely the bond lengths and electronic wave function parameters of the guest copper(II) complexes.

## 1. Introduction

The electron paramagnetic resonance (EPR sometimes labeled ESR) spectrum of  $\sim 0.3\%$  Cu doped into single crystals of  $(\text{NH}_4)_2[\text{M}(\text{NH}_3)_2(\text{CrO}_4)_2]$ ,  $\text{M} = \text{Cd}$  or  $\text{Zn}$ , was reported recently.<sup>1</sup> Similar behavior was observed in both hosts. Above  $\sim 300$  K the spectrum corresponded to g- and hyperfine A-tensors with close to axial symmetry. It was noted that this

is consistent with the crystal structure reported<sup>2</sup> for the zinc host lattice, in which all four Zn–O bonds to the chromate oxygen atoms of the  $\text{Zn}(\text{NH}_3)_2\text{O}_4$  units are crystallographically equivalent. However, below  $\sim 300$  K a transition to a phase giving rise to orthorhombic g- and A-tensors occurred, and it was inferred that this involves a triclinic unit cell. It was suggested that at high temperature the ammine groups freely rotate and that the transition to the triclinic phase is probably associated with the “locking” of the ammonia hydrogen atoms into particular positions in the lattice. Moreover, in the low-temperature phase, two of the g- and A-values were observed

\* Address correspondence to this author.

<sup>†</sup> Crystallography Laboratory.

<sup>‡</sup> Department of Molecular Spectroscopy.

<sup>⊗</sup> Abstract published in *Advance ACS Abstracts*, September 1, 1995.

(1) Wang, D. M.; Kovacic, I.; Reijerse, E. J.; de Boer, E. J. *Chem. Phys.* 1992, 97 (6), 3897.

(2) Harel, M.; Knobler, C.; McCullough, J. D. *Inorg. Chem.* 1969, 8, 11.



to vary with temperature, and it was concluded that this might be associated with "hopping" of the ammonia hydrogen atoms from one position to another.

The behavior of the EPR spectrum in the two phases is reminiscent of that exhibited by Cu<sup>2+</sup> doped into other lattices involving hydrogen-bonding groups such as NH<sub>4</sub><sup>+</sup>, NH<sub>3</sub>, and H<sub>2</sub>O. For example, the species Cu(NH<sub>3</sub>)<sub>2</sub>Cl<sub>4</sub><sup>2-</sup>, Cu(H<sub>2</sub>O)<sub>2</sub>Cl<sub>4</sub><sup>2-</sup>, and Cu(NH<sub>3</sub>)(H<sub>2</sub>O)Cl<sub>4</sub><sup>2-</sup> are formed when Cu<sup>2+</sup> is doped into NH<sub>4</sub>Cl under different conditions, and the temperature dependence of the EPR spectra of these have been the subject of numerous studies.<sup>3,4</sup> The host lattice undergoes a phase transition involving the "locking" of the hydrogen atoms of the NH<sub>4</sub><sup>+</sup> ions into specific positions at ~250 K, and the EPR spectra of the guest Cu<sup>2+</sup> centers have been used as a probe of this change.<sup>3</sup> The spectrum of Cu<sup>2+</sup> in the monoclinic phase of (NH<sub>4</sub>)<sub>2</sub>[Cd(NH<sub>3</sub>)<sub>2</sub>(CrO<sub>4</sub>)<sub>2</sub>] is very similar to those of the Cu(H<sub>2</sub>O)<sub>2</sub>Cl<sub>4</sub><sup>2-</sup> and Cu(NH<sub>3</sub>)(H<sub>2</sub>O)Cl<sub>4</sub><sup>2-</sup> centers at high temperature.<sup>4</sup> Moreover, the Tutton salt (NH<sub>4</sub>)<sub>2</sub>[Cu(H<sub>2</sub>O)<sub>6</sub>](SO<sub>4</sub>)<sub>2</sub> exhibits a temperature-dependent EPR spectrum due to a dynamic equilibrium between two forms which differ in the direction of the long axis of the Jahn–Teller distorted Cu(H<sub>2</sub>O)<sub>6</sub><sup>2+</sup> ions,<sup>5</sup> and the direction of this distortion exhibits a pressure-dependent "switch" upon deuteration associated with a change in the hydrogen-bonding network in the lattice.<sup>6</sup> The temperature dependence of the spectrum of Cu<sup>2+</sup> in the triclinic phase of (NH<sub>4</sub>)<sub>2</sub>[Cd(NH<sub>3</sub>)<sub>2</sub>(CrO<sub>4</sub>)<sub>2</sub>] is quite similar to that of (NH<sub>4</sub>)<sub>2</sub>[Cu(H<sub>2</sub>O)<sub>6</sub>](SO<sub>4</sub>)<sub>2</sub>. The EPR spectra of the copper(II) Tutton salts and Cu<sup>2+</sup>-doped NH<sub>4</sub>Cl have been interpreted satisfactorily using a model based upon dynamic vibronic coupling,<sup>4,6,7</sup> so it was of interest to apply this approach to the spectra of Cu<sup>2+</sup>-doped (NH<sub>4</sub>)<sub>2</sub>[Cd(NH<sub>3</sub>)<sub>2</sub>(CrO<sub>4</sub>)<sub>2</sub>]. In addition, the structure of the host cadmium(II) compound was determined both above and below the phase transition, and the present paper describes the results of these studies.

## 2. Experimental Section

**2.1. Preparation of Compounds and Optical and EPR Measurements.** The preparation and characterization of the crystals of (NH<sub>4</sub>)<sub>2</sub>[Cd(NH<sub>3</sub>)<sub>2</sub>(CrO<sub>4</sub>)<sub>2</sub>] have been described previously.<sup>1</sup> A sample of (NH<sub>4</sub>)<sub>2</sub>[Cu(NH<sub>3</sub>)<sub>2</sub>(CrO<sub>4</sub>)<sub>2</sub>] was also prepared by previously reported methods. (Anal. Found: N, 15.38; H, 3.88. Calc for CuN<sub>4</sub>H<sub>14</sub>Cr<sub>2</sub>O<sub>8</sub>: N, 15.32; H, 3.86.<sup>8</sup>) The electronic reflectance spectrum was recorded using a Beckmann DKA spectrophotometer. The EPR spectrum was measured using a JEOL JES-FE spectrometer operating at Q-band (~36 GHz) frequency.

**2.2. X-ray Diffraction Measurements.** As already reported,<sup>1</sup> the title compound exists in two crystal forms, a high-temperature modification and a low-temperature modification, the transition temperature between these being 300 ± 2 K = 27 °C. The structures of these were investigated in two independent studies. In one of these (by J.M.M.S. and P.T.B.) X-ray diffraction data were collected above the transition point at 320 ± 2 K = 47 °C (this structure is denoted CHROMH) and below this point at 250 ± 2 K = -23 °C (denoted CHROML(A)). These temperatures were set by leading a flow of heated or cooled nitrogen gas over the crystal, the temperature of which could be kept constant within at least 2°.

The transition point was passed by slowly increasing or decreasing the temperature in steps of 1° over a period of about 1 h. However,

**Table 1.** Crystallographic Data for CHROMH, CHROML(A), and CHROML(B)

	CHROMH	CHROML(A)	CHROML(B)
chem formula	(NH <sub>4</sub> ) <sub>2</sub> [Cd(NH <sub>3</sub> ) <sub>2</sub> (CrO <sub>4</sub> ) <sub>2</sub> ]		
<i>a</i> , Å	12.8380(11)	6.0210(4)	6.031(1)
<i>b</i> , Å	6.0308(6)	7.0363(4)	7.090(1)
<i>c</i> , Å	7.5890(6)	7.5714(8)	7.609(1)
α, deg	90	106.802(18)	107.73(1)
β, deg	110.154(14)	93.032(12)	91.19(1)
γ, deg	90	114.079(11)	114.64(1)
<i>V</i> , Å <sup>3</sup>	551.6	274.9	277.6(1)
<i>Z</i>	2	1	1
fw		250.545(8)	
space group	<i>C</i> 2/ <i>m</i> (No. 12)	<i>P</i> 1̄ (No. 2)	<i>P</i> 1̄ (No. 2)
temp, °C	47(2)	-23(2)	20(2)
λ, Å		0.71073	
<i>Q</i> <sub>calc</sub> , g cm <sup>-3</sup>	2.496	2.504	2.480
μ, cm <sup>-1</sup>	38.38	38.26	38.0
<i>R</i> ( <i>F</i> <sub>o</sub> ) <sup>a</sup>	0.0248	0.0547	0.0354
<i>R</i> <sub>w</sub> ( <i>F</i> <sub>o</sub> ) <sup>b</sup>	0.0280	0.0817	0.0433

<sup>a</sup> *R*(*F*<sub>o</sub>) = Σ||*F*<sub>o</sub> - |*F*<sub>c</sub>||/Σ|*F*<sub>o</sub>|. <sup>b</sup> *R*<sub>w</sub>(*F*<sub>o</sub>) = Σ*w*||*F*<sub>o</sub> - |*F*<sub>c</sub>||/Σ*w*|*F*<sub>o</sub>|. *w* = (σ<sup>2</sup>(*F*<sub>o</sub>) + *q*|*F*<sub>o</sub>|<sup>2</sup>)<sup>-1</sup>, where *q* = 0.00015 (CHROMH and CHROML(A)) and *q* = 0.0 (CHROML(B)).

experiments showed that it took considerably longer for the crystal to complete the transition. Peak positions found shortly after the new temperature was set shifted considerably during the following hours. Therefore it was necessary to wait overnight before a new stable situation was reached. This behavior was observed in both directions of the temperature change. After the temperature had stabilized for CHROMH, good quality data were collected. Peak profiles were only slightly broadened (width about 1.2°) and a good fit was found between observed and calculated peak positions. The solution of the crystal structure of CHROMH was easy, straightforward, and reasonably accurate, with a final *R* = 2.5% and *R*<sub>w</sub> = 2.8%. After lowering of the temperature, the same bad quality data returned showing that the process is reversible.

Data collected for the low-temperature form showed that CHROML(A) was severely twinned/disordered, and although the basic structure could be solved without difficulty, the accuracy was low (*R* = 11%) and no hydrogen atoms could be found for this data set. Therefore a new batch of crystals was prepared and a crystal which had been kept well below the transition temperature all the time was selected to collect the data. Although these data are considerably better, they still lack the quality of the high-temperature data. This crystal showed only slightly broadened profiles (width about 1.2°), and a good fit was found between observed and calculated peak positions. The solution of the crystal structure of CHROML(A) was easy and straightforward, with a final *R* = 5.5% and *R*<sub>w</sub> = 8.2%. Experimental details of these two structure determinations are given in Table 1 and Supporting Information Table S2.

In the second structure determination (by B.M.G., G.B.D., and G.N.W.), a batch of crystals was prepared and studied at 293 K. No evidence of twinning or disorder was apparent and the structure proved to be that of the low-temperature form of the compound. Solution of the structure, hereafter labeled CHROML(B), proved straightforward with final *R*-factors *R* = 2.93% and *R*<sub>w</sub> = 3.53%. Details of this determination are presented in Table 1.

## 3. Results and Discussion

**3.1. Crystal Structures.** Atomic positions for CHROMH and CHROML(A) and -(B) are listed in Table 2, and bond lengths and angles are given in Tables 3 and 4. Possible hydrogen bonding interactions and thermal parameters for CHROMH and CHROML(A) are detailed as Supporting Information Tables S3 and S4.

The unit cell of the high-temperature modification giving the labeling of the atoms, viewed down the *c* axis, is shown in Figure 1A. As reported previously,<sup>1</sup> in its high-temperature form, (NH<sub>4</sub>)<sub>2</sub>[Cd(NH<sub>3</sub>)<sub>2</sub>(CrO<sub>4</sub>)<sub>2</sub>] is isostructural with the analogous zinc(II) complex, and the coordination about the Cd<sup>2+</sup> ion

(3) Pilbrow, J. R.; Spaeth, J. M. *Phys. Stat. Solidi B* 1967, 20, 225. Kuroda, N.; Kawamori, A. *J. Phys. Chem. Solids* 1971, 32, 1233.

(4) Riley, M. J.; Hitchman, M. A.; Reinen, D.; Steffen, G. *Inorg. Chem.* 1988, 27, 1924.

(5) Alcock, N. W.; Duggan, M.; Murray, A.; Tyagi, S.; Hathaway, B. J.; Hewat, A. W. *J. Chem. Soc., Dalton Trans.* 1984, 7.

(6) Simmons, C. J.; Hitchman, M. A.; Stratemeier, H.; Schultz, A. J. *J. Am. Chem. Soc.* 1993, 115, 11304.

(7) Riley, M. J.; Hitchman, M. A.; Reinen, D. *Chem. Phys.* 1986, 102, 11.

(8) Gatehouse, B. M.; Guddat, L. W. *Acta Crystallogr.* 1987, C43, 14455.



**Table 2.** Atomic Positions and Thermal Parameters ( $\text{\AA}^2$ ) for **CHROMH**, **CHROML(A)**, and **CHROML(B)**

CHROMH				
atom	<i>x</i>	<i>y</i>	<i>z</i>	<i>B</i> <sub>eq</sub> <sup>a</sup>
Cd(1)	0.00000	0.00000	0.00000	0.95(1)
Cr(1)	0.15769(4)	0.50000	0.22104(7)	0.77(2)
O(1)	0.1399(2)	0.2757(3)	0.0875(3)	1.83(6)
O(2)	0.0705(2)	0.50000	0.3362(4)	1.93(9)
O(3)	0.2842(2)	0.50000	0.3689(4)	2.60(10)
N(1)	0.0006(3)	0.00000	0.2894(5)	1.92(11)
N(2)	0.3298(3)	0.00000	0.2597(5)	1.70(11)
H(11)	-0.049(4)	0.0000	0.308(7)	3.(2)
H(12)	0.035(3)	0.103(6)	0.353(5)	3.7(12)
H(21)	0.377(6)	0.0000	0.232(9)	6.(2)
H(22)	0.348(4)	0.0000	0.385(7)	1.1(11)
H(23)	0.292(4)	0.110(8)	0.220(6)	6.(2)
CHROML(A)				
atom	<i>x</i>	<i>y</i>	<i>z</i>	<i>B</i> <sub>eq</sub> <sup>a</sup>
Cd(1)	0.00000	0.00000	0.00000	1.66(1)
Cr(1)	0.66943(10)	0.31470(8)	0.22049(7)	1.52(2)
O(1)	0.4189(5)	0.2689(5)	0.0796(4)	2.54(9)
O(2)	0.8772(5)	0.2877(4)	0.0925(4)	2.25(9)
O(3)	0.5942(6)	0.1384(5)	0.3369(4)	2.50(9)
O(4)	0.7855(7)	0.5671(5)	0.3681(5)	2.97(10)
N(1)	0.0299(7)	-0.0019(5)	0.2912(4)	2.60(11)
N(2)	0.6565(7)	0.3409(5)	0.7386(5)	2.43(10)
H(11)	0.2063(7)	0.0927(5)	0.3594(4)	
H(12)	-0.0223(7)	-0.1553(5)	0.2928(4)	
H(13)	-0.0777(7)	0.0599(5)	0.3578(4)	
H(21)	0.5879(7)	0.1937(5)	0.7487(5)	
H(22)	0.6453(7)	0.3284(5)	0.6039(5)	
H(23)	0.8355(7)	0.4268(5)	0.8036(5)	
H(24)	0.5611(7)	0.4221(5)	0.7979(5)	
CHROML(B)				
	<i>x</i>	<i>y</i>	<i>z</i>	$10^3 U_{eq}$ <sup>b</sup>
Cd	0.00000	0.00000	0.00000	2.00(2)
Cr	0.66271(10)	0.31531(9)	0.22100(8)	1.81(2)
O(1)	0.4164(5)	0.2751(5)	0.0847(4)	2.94(1)
O(2)	0.8697(5)	0.2827(5)	0.0899(4)	2.72(1)
O(3)	0.5819(6)	0.1414(5)	0.3370(4)	2.86(1)
O(4)	0.7848(6)	0.5683(5)	0.3684(4)	3.58(1)
N(1)	0.0119(7)	-0.0010(6)	0.2893(5)	2.94(1)
N(2)	0.6651(6)	0.3385(5)	0.7402(5)	2.75(1)
H(11)	0.2047(7)	0.0582(6)	0.2679(5)	
H(12)	0.1535(7)	0.0313(6)	0.3779(5)	
H(13)	-0.0420(7)	0.0840(6)	0.3587(5)	
H(21)	0.6011(6)	0.1686(5)	0.7614(5)	
H(22)	0.6541(6)	0.2934(5)	0.6147(5)	
H(23)	0.8315(6)	0.4324(5)	0.7842(5)	
H(24)	0.6119(6)	0.4301(5)	0.7817(5)	

$$^a B_{eq} = 8\pi^2(U_{11} + U_{22} + U_{33})/3. \quad ^b U_{eq} = 1/3 \sum_{ij} U_{ij} a_i^* a_j^* a_i a_j.$$

and packing of the anions and cations is as already described<sup>2</sup> in detail for that compound. The coordination geometry about the  $\text{Cd}^{2+}$  is close to an ideal octahedron, all metal–ligand bond angles being within  $\sim 1.2^\circ$  of  $90^\circ$ . The equivalent *trans* Cd–NH<sub>3</sub> bonds lie close to the *c* crystal axis, as may be seen from the projection of the unit cell viewed along *b* shown in Figure 1B. Of particular relevance to the EPR spectrum (see section 3.2) is the fact that all four Cd–O bonds to chromate oxygen atoms, which lie approximately in the (001) plane, are crystallographically equivalent.

The structures revealed by the two determinations (A) and (B) of the low-temperature form of  $(\text{NH}_4)_2[\text{Cd}(\text{NH}_3)_2(\text{CrO}_4)_2]$  are essentially identical, all parameters agreeing to within about 3 standard deviations (Tables 1 and 3 and 4). As predicted from the EPR spectrum of the  $\text{Cu}^{2+}$ -doped complex,<sup>1</sup> the low-temperature form has a triclinic cell, and after allowance for an interchange of the *a* and *c* axes and  $\alpha$  and  $\beta$  angles, the

**Table 3.** Geometrical Data for **CHROMH** and **CHROML(A)**

CHROMH		CHROML(A)
Bond Lengths (Å)		
Cd—O1	2.368(2)	2.360(3) 2.359(3)
Cd—N1	2.194(3)	2.219(3)
Cr—O1	1.658(2)	1.681(3)
Cr—O2	1.640(3)	1.642(3)
Cr—O3	1.625(3)	1.660(3) 1.620(3)
Bond Angles (deg)		
O1—Cd—N1	88.8(1)	87.6(1) 91.0(1)
O1—Cd—O1	90.8(1)	89.5(1)
O1—Cr—O2	110.5(1)	109.0(2)
O1—Cr—O3	108.5(1)	111.0(2)
O2—Cr—O3	109.6(1)	110.1(1)
O1—Cr—O1'	109.3(1)	108.5(2) 108.7(2) 109.6(2)
Cd—O1—Cr	132.5(1)	134.2(2) 130.4(1)
H Bonds (Calcd)		
N1—H11	0.703(54)	
N1—H12	0.817(35)	
N2—H21	0.712(73)	
N2—H22	0.899(45)	
N2—H23	0.818(48)	

**Table 4.** Geometrical Data for **CHROML(B)**<sup>a</sup>

Bond Lengths ( $\text{\AA}$ )			
Cd–O	2.359(2)	N(1)–H(12)	0.977
Cd–N(1)	2.203(4)	N(1)–H(13)	0.851
Cr–O(1)	1.663(3)	N(2)–H(21)	1.166
Cr–O(2)	1.661(3)	N(2)–H(22)	0.901
Cr–O(3)	1.648(4)	N(2)–H(23)	0.925
Cr–O(4)	1.630(3)	N(2)–H(24)	0.823
Bond Angles (deg)			
O(1)–Cd–N(1)	88.8(1)	O(2)–Cr–O(3)	110.4(2)
	91.2(1)	O(1)–Cr–O(4)	108.4(2)
O(1)–Cd–O(1)'	180.0	O(3)–Cr–O(4)	109.6(2)
O(1)–Cr–O(2)'	109.3(2)	O(4)–Cr–O(2)'	108.7(1)
O(1)–Cr–O(3)	110.4(2)	Cd–O(1)–Cr	133.3(2)

<sup>a</sup> The hydrogen atoms were located in the difference Fourier synthesis and refined using a riding model with a common, fixed thermal parameter of  $0.08 \text{ \AA}^2$ .

compound is isomorphous with the corresponding copper(II) compound (unit cell parameters  $a = 7.362(2) \text{ \AA}$ ,  $b = 6.932(1) \text{ \AA}$ ,  $c = 5.895(1) \text{ \AA}$ ,  $\alpha = 112.39(3)^\circ$ ,  $\beta = 92.79(2)^\circ$ ,  $\gamma = 107.06(3)^\circ$ ).<sup>8</sup> An important change accompanying the high  $\rightarrow$  low temperature is the loss of the mirror plane normal to the *b* axis, which, in combination with the inversion center, requires all four Cd–O bonds to be crystallographically equivalent in the monoclinic cell. The projection of the unit cell viewed along  $a^*$  and showing the atomic numbering system is shown in Figure 1C. In the triclinic cell, the only symmetry element of the  $\text{Cd}^{2+}$  coordination polyhedron is an inversion center. In marked contrast to the corresponding copper(II) complex,<sup>8</sup> where the metal–oxygen bonds are very different in length ( $2.022(2)$  and  $2.425(1) \text{ \AA}$ ), those in the cadmium(II) compound are equal within experimental uncertainty ( $2.360(3)$  and  $2.359(3) \text{ \AA}$  in **CHROML(B)** with both being  $2.369(5) \text{ \AA}$  in **CHROML(A)**). However, the lowering in symmetry of the host compound which accompanies the phase transition has a marked effect upon the EPR spectrum of the guest  $\text{Cu}^{2+}$  complex (see section 3.2).

The relationship between the high- and low-temperature unit cells may be seen clearly by comparing the views shown in Figures 1B,C. As noted above, the X-ray patterns of crystals



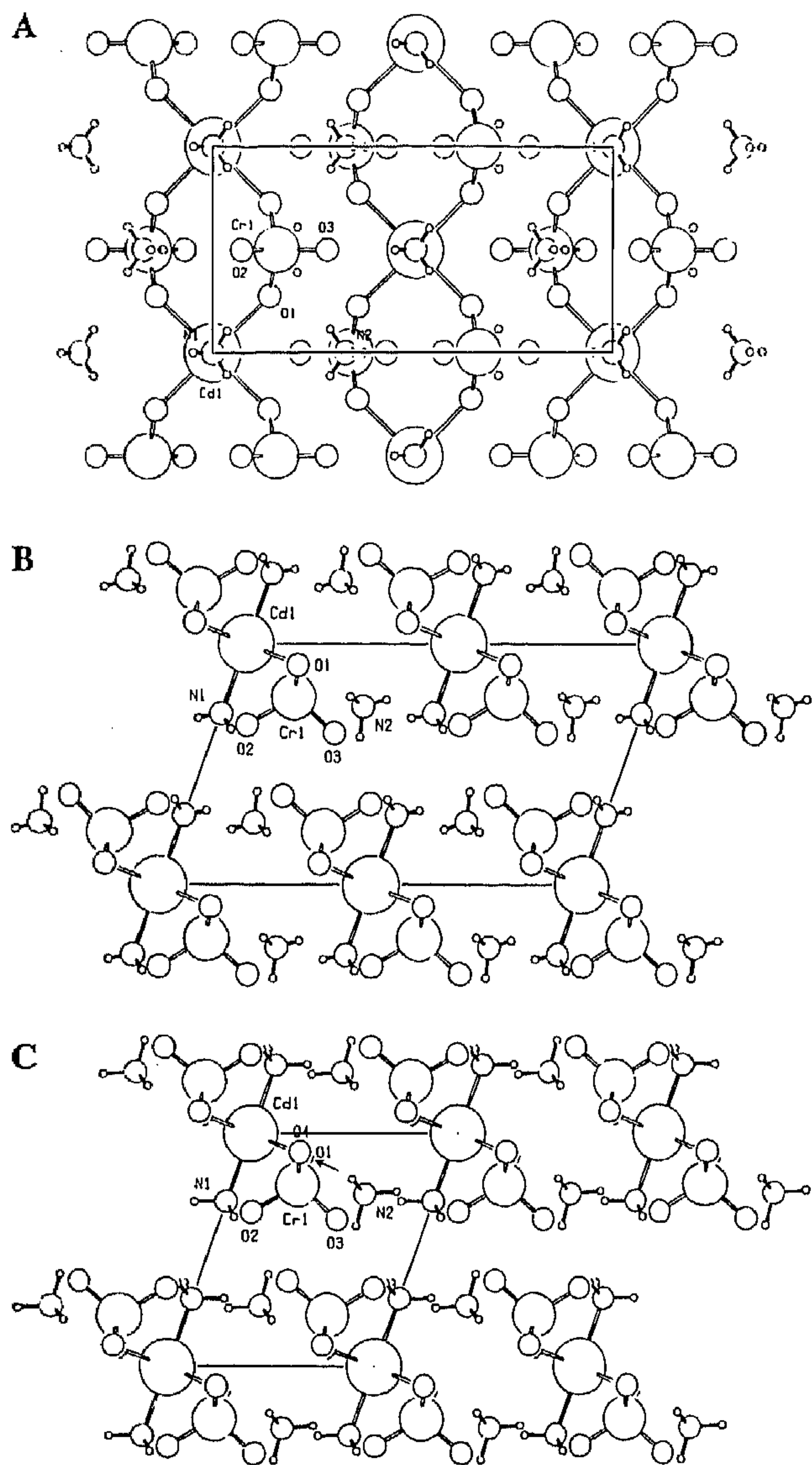


**Figure 1.** Unit cell with atomic numbering of the structure of (NH<sub>4</sub>)<sub>2</sub>[Cd(NH<sub>3</sub>)<sub>2</sub>(CrO<sub>4</sub>)<sub>2</sub>]. The numbering of the H and N atoms is omitted for clarity; N1 is part of the NH<sub>3</sub> ligand, while N2 belongs to the NH<sub>4</sub><sup>+</sup> ion. (a) High-temperature monoclinic cell projected along *c* on the *a\*b\** plane, origin lower left, *a* to the right, *b* up. (b) High-temperature monoclinic cell projected along *b* on the *ac* plane, origin upper left, *a* to the right *c* down. The atom O1 projects on top of the mirror-related atom O1'. (c) Low-temperature triclinic cell projected along *a\** (which corresponds to the *b* axis of the monoclinic form) on the *bc* plane, origin to the upper left, *b* to the right, *c* down. The atom O4 does not project on top of the pseudo-symmetry-related atom O1 (indicated by an arrow). A possible twin can be defined by reflection of the unit cell with respect to this pseudo-mirror plane (*a*, *c*).

cooled from above to below the transition temperature showed evidence of strong twinning. Figure 1C shows the arrangement of just one twin with respect to the high-temperature cell shown in Figure 1B. The second twin would have the orientation generated by the mirror plane normal to the *b* axis in the high-temperature unit cell.

**3.2. Temperature Dependence of the EPR Spectrum of the Cu<sup>2+</sup>-Doped Compound.** The way in which the EPR spectrum of Cu<sup>2+</sup> doped into a single crystal of (NH<sub>4</sub>)<sub>2</sub>[Cd(NH<sub>3</sub>)<sub>2</sub>(CrO<sub>4</sub>)<sub>2</sub>] varies over the temperature range 4 to ~370 K has been described in detail elsewhere.<sup>1</sup> The reported spectra conform to the symmetry requirements of the host unit cells above and below the transition temperature. For the high-temperature monoclinic cell, a single crystal was observed, with the principal axes of the *g*- and hyperfine *A*-tensors being

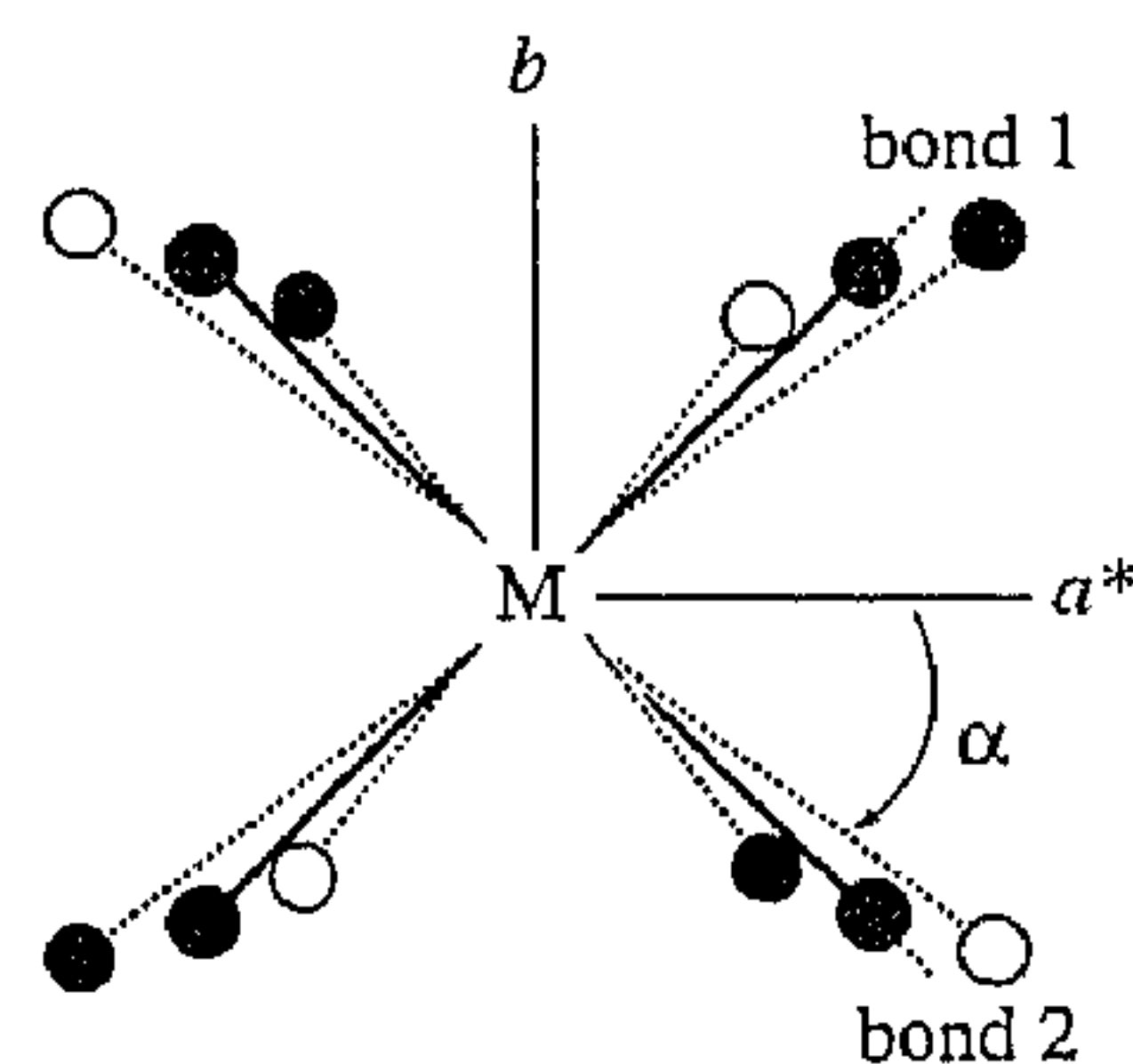


**Figure 2.** Schematic diagram showing the possible orientations of the guest copper(II) complexes in Cu<sup>2+</sup>-doped (NH<sub>4</sub>)<sub>2</sub>[Cd(NH<sub>3</sub>)<sub>2</sub>(CrO<sub>4</sub>)<sub>2</sub>] viewed down the *c* axis.

parallel to the *b*, *c*, and *a\** axes, as required by the symmetry elements of the Cd<sup>2+</sup> polyhedron (see preceding section). In this modification, the tensors have near tetragonal symmetry, with the two larger *g*-values being very similar (*g*<sub>1</sub> = 2.219(1), *g*<sub>2</sub> = 2.234(1), *g*<sub>3</sub> = 2.017(1)), and the spectra do not alter as a function of temperature. On cooling of the sample to below the transition temperature, the spectrum splits into two signals which have identical *g*- and *A*-tensors and show an angular dependence related by a mirror plane normal to the *b* axis. Each of these signals is clearly due to Cu<sup>2+</sup> doped into one of the symmetry-related twinned triclinic cells formed on cooling the monoclinic cell (see preceding section). The *g*- and *A*-tensors in the triclinic cell show a marked rhombic character, and the higher two *g*-values move apart as the temperature is lowered from ~200 to 4 K.

The behavior of the EPR spectrum of Cu<sup>2+</sup>-doped (NH<sub>4</sub>)<sub>2</sub>[Cd(NH<sub>3</sub>)<sub>2</sub>(CrO<sub>4</sub>)<sub>2</sub>] is rather similar to that of the complex Cu(H<sub>2</sub>O)<sub>2</sub>Cl<sub>4</sub><sup>2-</sup> formed when Cu<sup>2+</sup> is doped into the cubic lattice NH<sub>4</sub>Cl under conditions of low pH. Here, a tetragonal *g*-tensor is observed at higher temperatures (*g*<sub>1</sub> = *g*<sub>2</sub> = 2.292, *g*<sub>3</sub> = 2.019 at 130 K), but below ~40 K this transforms to an orthorhombic *g*-tensor (*g*<sub>1</sub> = 2.410, *g*<sub>2</sub> = 2.185, *g*<sub>3</sub> = 2.019).<sup>4</sup> Unlike the present system, the *g*-values below the transition temperature of Cu<sup>2+</sup>-doped NH<sub>4</sub>Cl do not vary significantly with temperature. However, this latter feature is exhibited by the EPR spectrum of the Cu(H<sub>2</sub>O)<sub>6</sub><sup>2+</sup> ion doped in a range of host lattices.<sup>9,10</sup> The behavior of both these systems has been explained by saying that, at the local level and to a first approximation, each copper(II) complex has a tetragonally elongated octahedral geometry with a slight orthorhombic distortion. The complex adopts two orientations in the crystal lattice which differ by interchange of the long and intermediate metal–ligand bonds. It is this aspect which gives rise to the unusual features observed in the EPR spectra of the compounds, and similar arguments may be used to provide a qualitative explanation of the EPR spectrum of Cu<sup>2+</sup>-doped (NH<sub>4</sub>)<sub>2</sub>[Cd(NH<sub>3</sub>)<sub>2</sub>(CrO<sub>4</sub>)<sub>2</sub>].

This model infers that the geometry of the guest complex is basically similar to that of pure (NH<sub>4</sub>)<sub>2</sub>[Cu(NH<sub>3</sub>)<sub>2</sub>(CrO<sub>4</sub>)<sub>2</sub>], with two long Cu–O bonds, two Cu–O bonds of intermediate length, and two short Cu–N bonds to the amine groups. The orientations of this in the cadmium host lattice are shown schematically in Figure 2 viewed down the *c* axis, which is parallel to the Cd–N bond direction. The long bonds of the guest copper(II) complex may be associated with either pair of the *trans* Cd–O bonds, and in the high-temperature monoclinic phase, these are crystallographically equivalent so that the two orientations, shown by the full and open circles on Figure 2, are equally probable (bond 1 ≡ bond 2). Exchange between

(9) Silver, B. L.; Getz, D. J. *J. Chem. Phys.* 1974, 61, 638.

(10) Riley, M. J.; Hitchman, Wan Mohammed, A. *J. Chem. Phys.* 1987, 87, 3766.



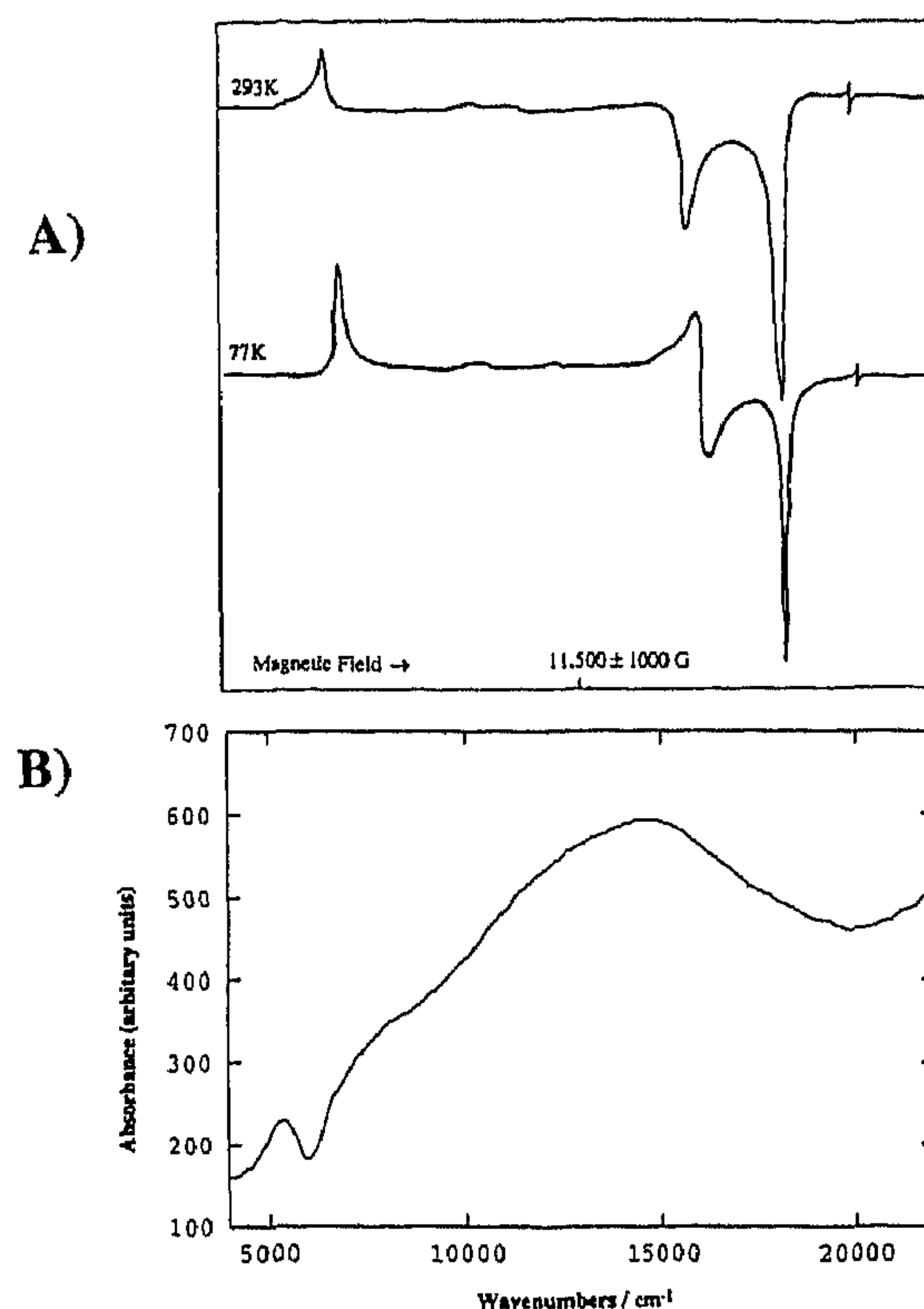


**Figure 3.** (A) EPR spectrum of powdered  $(\text{NH}_4)_2[\text{Cu}(\text{NH}_3)_2(\text{CrO}_4)_2]$  measured at  $Q$ -band frequency. The weak sharp peak at high field is due to a speck of powdered DPPH. (B) Reflectance spectrum of powdered  $(\text{NH}_4)_2[\text{Cu}(\text{NH}_3)_2(\text{CrO}_4)_2]$ .

them is rapid, so that they give rise to a single EPR signal. The equivalence of the two orientations means that the principal  $g$ -directions must lie along the  $a^*$  and  $b$  directions and the slight  $g$ -anisotropy may be explained by a small rotation of the Cu—O bond directions from those of the host cadmium complex.

On cooling to the sample to below  $\sim 300$  K, the principal directions of these higher  $g$ -values shift by  $\sim 45^\circ$ , from bisecting the Cd—O bond angles to lying close to the Cd—O bond directions. This is because in the low-temperature triclinic phase the Cd—O bonds are no longer crystallographically equivalent, so that the two orientations shown by the full and empty circles on the figure will differ in energy. The number of copper(II) complexes in each state will therefore depend upon the temperature. As exchange is still rapid on the EPR time scale, the observed spectrum will be the average of the forms, weighted by their relative populations, the principal  $g$ -axes will conform to those of the molecular  $g$ -tensors, and the spectrum will be temperature dependent. At 4 K, all the copper(II) complexes will adopt the lower energy orientation and the spectrum will be that of this molecular species. The EPR spectrum of powdered  $(\text{NH}_4)_2[\text{Cu}(\text{NH}_3)_2(\text{CrO}_4)_2]$  was recorded at 293 and 77 K (Figure 3A). The spectra show little change with temperature, and except for a somewhat smaller  $g_{\perp}$ -anisotropy the  $g$ -values (2.04, 2.08, 2.33) are quite similar to those of  $\text{Cu}^{2+}$ -doped  $(\text{NH}_4)_2[\text{Cd}(\text{NH}_3)_2(\text{CrO}_4)_2]$  at low temperature (2.02, 2.13, 2.30) as expected from this model. Although this cannot be determined experimentally, because it is impossible to tell which spectrum is associated with which sublattice in the twinned crystals, it seems reasonable that for the lower energy orientation the long bonds occur to the same atoms in the cadmium host as in the pure copper compound, namely O1, the orientation pictured by the full circles in Figure 2.

Assuming that the local molecular  $g$ -values in the high-temperature phase are similar to those derived from the spectrum at 4 K, the  $g$ -values along the  $a^*$  and  $b$  directions may be used

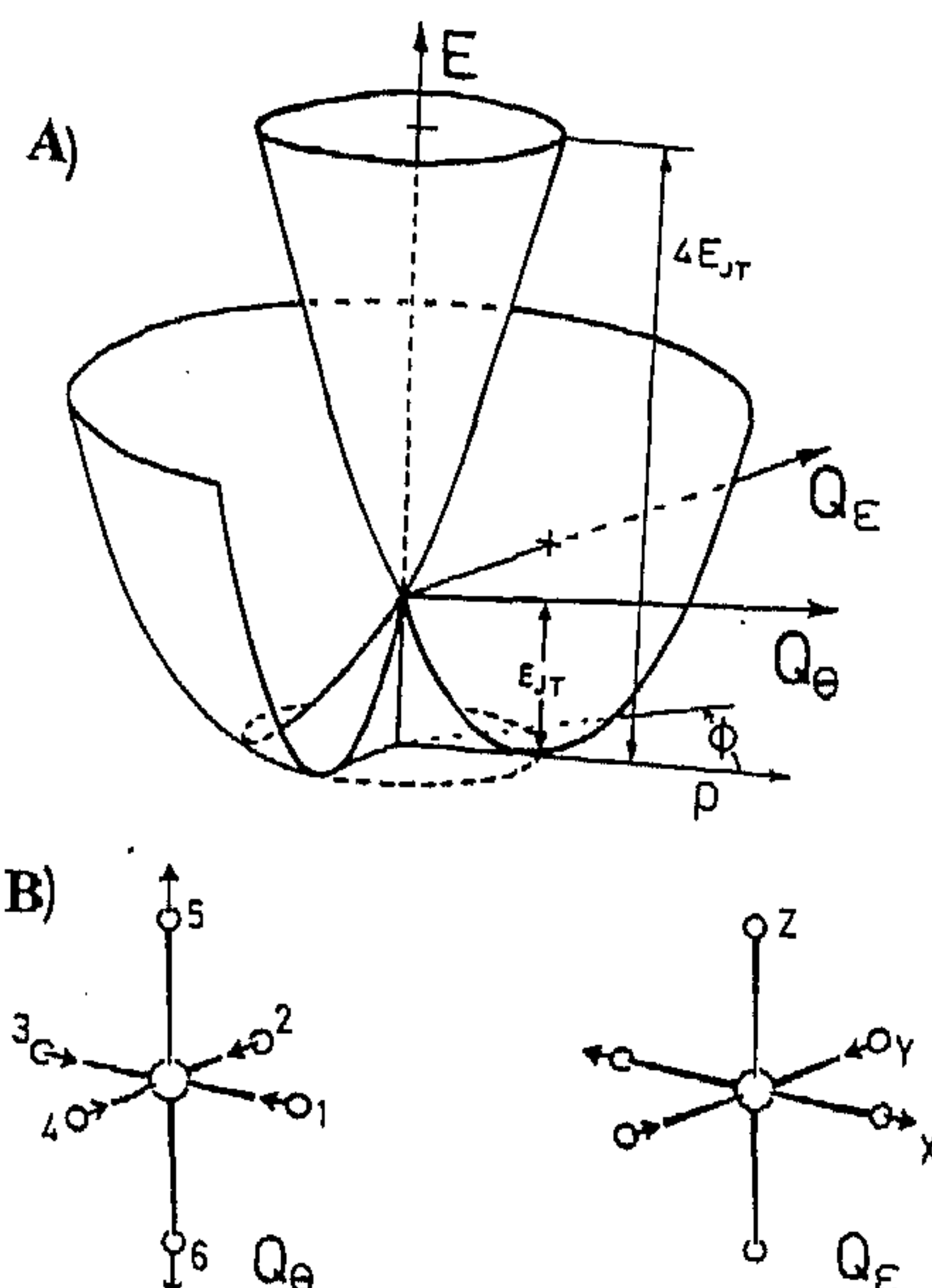


**Figure 4.** (A) "Mexican hat" potential surface formed by  $E_g \times e_g$  Jahn-Teller coupling. (B) Form of the two components of the Jahn-Teller active  $e_g$  vibration.

to estimate the orientation of the local  $g$ -axes. If these make an angle  $\alpha$  with the  $a^*$  direction as illustrated in Figure 2, then

$$g(a^*)^2 = g_y^2 \cos^2(\alpha) + g_x^2 \sin^2(\alpha)$$

$$g(b)^2 = g_y^2 \sin^2(\alpha) + g_x^2 \cos^2(\alpha)$$

$$[g(a^*)^2 - g(b)^2]/[g_y^2 - g_x^2] = \cos(2\alpha) \quad (1)$$

Substitution into (1) of the reported<sup>1</sup> values  $g(a^*) = 2.234$ ,  $g(b) = 2.219$ ,  $g_y = 2.298$ , and  $g_x = 2.129$  yields the estimate  $\alpha = 42^\circ$ . It may be noted that the Cd—O bonds make an angle of  $44.7^\circ$  with the  $a^*$  axis and that the observed angle between  $g_y$  and the  $a^*$  axis in the triclinic phase is  $47.5^\circ$  at 4.2 K but that this falls to  $44^\circ$  as the temperature rises to 200 K.<sup>1,11</sup>

A model of dynamic vibronic coupling which provides a more quantitative explanation of the temperature dependence of the EPR spectra of  $\text{Cu}^{2+}$  complexes has been reported,<sup>4,7,10</sup> and this will now be applied to the present system.

**3.2.1. Model of Dynamic Vibronic Coupling.** The energy levels of a copper(II) complex are conventionally described in terms of the coupling between the  $^2E_g$  electronic state and the  $e_g$  Jahn-Teller active vibration.<sup>12</sup> To 1st order, a complex with six identical ligands undergoes a radial distortion  $\rho$  in the  $e_g$  mode to yield the "Mexican hat" potential surface shown in Figure 4A. Here,  $E_{JT}$  represents the Jahn-Teller stabilization energy, with the splitting between the upper and lower portions of the potential surface being  $4E_{JT}$ . At this level of approximation, the  $Q_\theta$  and  $Q_\epsilon$  components of the vibration, pictured in Figure 4B, are equivalent, and the energy minimum is a circular well of radius  $\rho$  with the geometry and concomitant electronic wave function specified by the angle  $\phi$ . Higher order effects distort this surface, producing three minima which almost invariably occur at  $\phi = 0, 120$ , and  $240^\circ$ , corresponding to octahedral geometries tetragonally elongated along  $z$ ,  $x$ , and  $y$ , respectively, and the unpaired electron in a  $d_{x^2-y^2}$  type orbital. Saddlepoints corresponding to compressed tetragonal geometries, and  $d_z^2$  type electronic wave functions, occur at  $\phi = 60$ ,

(11) Wang, D. M. Unpublished results.

(12) Bersuker, I. B. *The Jahn-Teller Effect and Vibronic Interactions in Modern Chemistry*; Plenum Press: New York, 1984.



180, and 300°, the energy difference between the minima and saddlepoints being defined as  $2\beta$ . When the ligands are inequivalent, either inherently or due to interactions with the surrounding crystal lattice, this shifts both the positions and relative energies of the minima, and it is the dynamic equilibrium between the vibronic levels of such surfaces that gives rise to temperature-dependent effects of the kind discussed here.<sup>13</sup> The low-symmetry components of the metal–ligand interaction are normally expressed by a “strain” characterized by axial and equatorial components  $S_\theta$  and  $S_e$ , respectively. This model has been able to account quantitatively for the temperature dependence of the EPR spectra and geometries of a range of dynamic copper(II) complexes<sup>14</sup> and may be applied to the present system in the following manner.

**3.2.2. Potential Surface of the Copper(II) Complex.** The procedure used to calculate the potential surface of a copper(II) complex under the influence of Jahn–Teller coupling and an orthorhombic strain has been described in detail previously.<sup>4,7,10</sup> For the present system, the basic potential surface of the Cu(NH<sub>3</sub>)<sub>2</sub>O<sub>4</sub> unit formed upon doping Cu<sup>2+</sup> into (NH<sub>4</sub>)<sub>2</sub>[Cd(NH<sub>3</sub>)<sub>2</sub>(CrO<sub>4</sub>)<sub>2</sub>] is best defined by considering the  $g$ -values at low temperature. The temperature dependence of the  $g$ -values, and the way in which they alter with the phase transition of the host, is then used to define the effects of the interaction with the surrounding lattice. Although the metal hyperfine parameters may in principle be treated in a similar fashion, the interpretation is complicated by the fact that these depend not only on the orbital angular momentum of the unpaired electron but also on the “contact” interaction between the  $s$ -electron density and the nuclear spin. Since the primary interest is in the dynamics of the system, the hyperfine coupling has therefore not been considered in the present treatment.

The overall Jahn–Teller distortion is largely decided by the balance between the force constant of the  $e_g$  mode and the linear coupling constant  $A_1$ . For the present complex the former was assumed to be similar to that reported<sup>10</sup> for the Cu(H<sub>2</sub>O)<sub>6</sub><sup>2+</sup> ion, where  $h\nu = 300\text{ cm}^{-1}$ . This seems reasonable, given the similarities of the ligand donor atoms. The value of  $A_1$  may be obtained from the relationship (see refs 7 and 12 for a discussion of the various parameters and the units used to define them)

$$A_1 = (2h\nu E_{JT})^{1/2} \quad (2)$$

The Jahn–Teller stabilization energy  $E_{JT}$  (Figure 4A) is approximately related to the energy  $\Delta E$  of the transition between the split levels of the  $^2E_g$  state of the parent octahedral complex by the expression

$$\Delta E \approx 4E_{JT} + 2|S_\theta| \quad (3)$$

Here, the basic splitting between the upper and lower portions of the surface ( $4E_{JT}$ ) is modified by the effect of the strain.<sup>13,15</sup> The reflectance spectrum of (NH<sub>4</sub>)<sub>2</sub>[Cu(NH<sub>3</sub>)<sub>2</sub>(CrO<sub>4</sub>)<sub>2</sub>] is shown in Figure 3B. This consists of a band at 14 000 with a shoulder at  $\sim 12\,000\text{ cm}^{-1}$ , which may be assigned to transitions to the split components of the  $^2T_{2g}$  level of the parent octahedral complex, and a shoulder at  $\sim 8300\text{ cm}^{-1}$ , which is due to the transition between the levels derived from the  $d_{x^2-y^2}$  and  $d_{z^2}$  orbitals. The sharp peak at  $\sim 5000\text{ cm}^{-1}$  is assigned as an infrared overtone. Substitution of  $\Delta E = 8300\text{ cm}^{-1}$  into (3) and anticipating the value  $S_\theta \approx -1000\text{ cm}^{-1}$  give  $E_{JT} = 1575\text{ cm}^{-1}$ , and substitution of this into eq 2 yields the estimate  $A_1 = 975\text{ cm}^{-1}$ . This is slightly larger than the value of  $900\text{ cm}^{-1}$

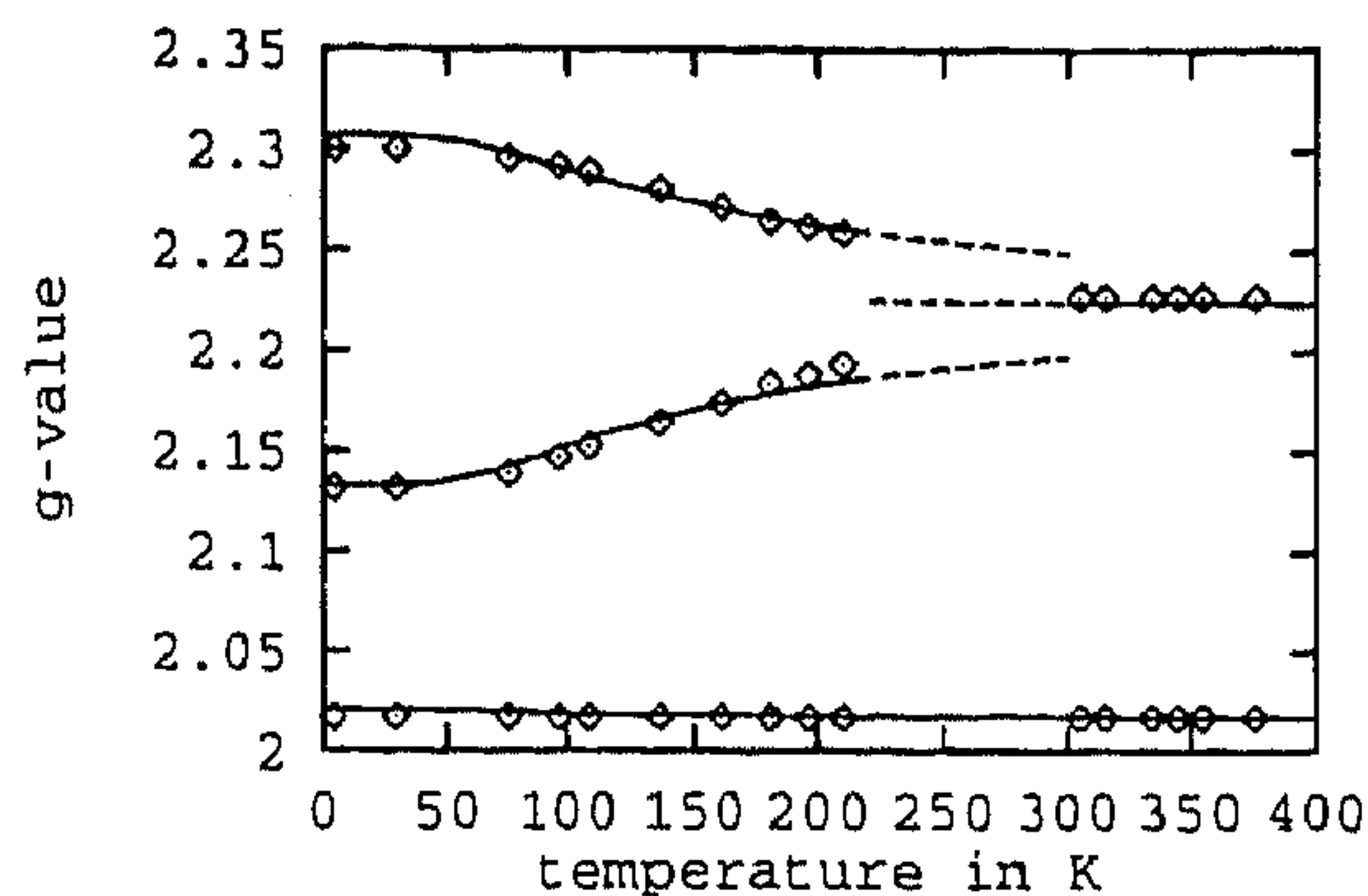


**Figure 5.** Calculated variation of the  $g$ -values of Cu<sup>2+</sup>-doped (NH<sub>4</sub>)<sub>2</sub>[Cd(NH<sub>3</sub>)<sub>2</sub>(CrO<sub>4</sub>)<sub>2</sub>] for the high ( $>300\text{ K}$ ) and low ( $<300\text{ K}$ ) temperature phases of the host lattice (lines). See text for the method of calculation; experimental points are shown as symbols.

reported<sup>10</sup> for the Cu(H<sub>2</sub>O)<sub>6</sub><sup>2+</sup> ion, possibly reflecting the slightly stronger ligand field of NH<sub>3</sub> compared with H<sub>2</sub>O.

For the present complex, the strain will be dominated by the difference in  $\sigma$ -bonding strength of the *trans* ammonia ligands and the in-plane chromate oxygen atoms. Assuming that the ligand field of the latter is not too different from water, which seems reasonable since oxygen-donor ligands consistently lie considerably lower in the spectrochemical series than ammonia,<sup>16</sup> this may be estimated from the strain parameters derived for the centers Cu(H<sub>2</sub>O)<sub>2</sub>Cl<sub>4</sub><sup>2-</sup> and Cu(NH<sub>3</sub>)<sub>2</sub>Cl<sub>4</sub><sup>2-</sup> formed when Cu<sup>2+</sup> is doped into NH<sub>4</sub>Cl. Here,  $S_\theta = -200\text{ cm}^{-1}$  for the former, and  $-1200\text{ cm}^{-1}$  for the latter,<sup>4</sup> implying a difference between the NH<sub>3</sub> and H<sub>2</sub>O ligands corresponding to  $S_\theta = -1000\text{ cm}^{-1}$ .

The position of the minimum in the “trough” of the warped Mexican hat potential surface depends upon the balance between the strain, which in the present case favors a compressed tetragonal geometry, and the warping parameter  $\beta$ , which is a measure of the tendency of the strain-free complex to prefer a tetragonally elongated geometry. It has been shown<sup>17</sup> that the former geometry will only become stable when  $|S_\theta| > \sim 9\beta$ . An axially symmetric strain of lower magnitude, relative to  $\beta$ , will produce a pair of equivalent minima each corresponding to an orthorhombic geometry.<sup>17</sup> The calculation of the low-temperature orthorhombic  $g$ -tensor of Cu<sup>2+</sup>-doped (NH<sub>4</sub>)<sub>2</sub>[Cd(NH<sub>3</sub>)<sub>2</sub>(CrO<sub>4</sub>)<sub>2</sub>] thus provides a means of estimating the ratio of  $S_\theta$  to  $\beta$  quite accurately. In the triclinic modification, the low symmetry of the host lattice will impose an orthorhombic component  $S_e$  to the strain acting upon the guest copper(II) complex. This causes the two orthorhombic geometries of the copper(II) complex to become inequivalent in energy. As the separation between these is comparable to thermal energies, the two higher  $g$ -values are temperature dependent, and modeling this aspect allows  $S_e$  to be estimated. It should be noted that the temperature invariance of the lowest  $g$ -value over the range 4–370 K shows that the upper well in the warped potential surface, which corresponds to the long bonds occurring to the ammonia ligands, is significantly higher than the thermal energies involved, and this provides a lower limit of  $\sim -400\text{ cm}^{-1}$  for the parameter  $S_\theta$ .

The temperature dependence of the  $g$ -values of Cu<sup>2+</sup>-doped (NH<sub>4</sub>)<sub>2</sub>[Cd(NH<sub>3</sub>)<sub>2</sub>(CrO<sub>4</sub>)<sub>2</sub>] in the range 4–300 K were calculated for a wide range of values of  $\beta$  and  $S_e$  by the procedure described in detail elsewhere.<sup>10</sup> Optimum agreement with experiment was obtained using the values  $\beta = 240\text{ cm}^{-1}$  and  $S_e = 140\text{ cm}^{-1}$ , the fit being shown in Figure 5. Orbital reduction parameters

(13) Reinen, D.; Atanasov, M. *Magn. Reson. Rev.* **1991**, *15*, 167.

(14) Hitchman, M. A. *Comments Inorg. Chem.* **1994**, *15*, 197.

(15) Reinen, D.; Friebe, C. *Struct. Bonding (Berlin)* **1979**, *37*, 1.

(16) Lever, A. B. P. *Inorganic Electronic Spectroscopy*, 2nd ed.; Elsevier: New York, 1984; Chapter 6.

(17) Reinen, D.; Krause, S. *Inorg. Chem.* **1981**, *20*, 2750.



**Table 5.** Composition of the Vibrational and Electronic Components of the Four Lowest Energy Vibronic Wave Functions Calculated for the Potential Surface of Cu<sup>2+</sup>-Doped (NH<sub>4</sub>)<sub>2</sub>[Cd(NH<sub>3</sub>)<sub>2</sub>(CrO<sub>4</sub>)<sub>2</sub>] in the High-Temperature Monoclinic and Low-Temperature Triclinic Phases<sup>a</sup>

energy (cm <sup>-1</sup> )	bond lengths (Å)			electronic wave function			g-values		
	Cu—O	Cu—O	Cu—N	$\langle c^2 \rangle$	$\langle e^2 \rangle$	$\langle f^2 \rangle$	$g_1$	$g_2$	$g_3$
High-Temperature Monoclinic Phase									
226	2.22	2.23	1.97	1.25	1.22	3.54	2.207	2.240	2.019
138	2.23	2.22	1.97	1.11	1.22	3.68	2.219	2.239	2.011
20	2.17	2.28	1.97	1.61	0.70	3.56	2.165	2.291	2.017
0	2.28	2.17	1.97	0.64	1.74	3.62	2.261	2.189	2.014
Low-Temperature Triclinic Phase									
293	2.31	2.13	1.98	0.38	2.15	3.47	2.286	2.150	2.022
193	2.24	2.21	1.97	1.11	1.33	3.56	2.219	2.229	2.017
145	2.21	2.25	1.96	1.36	0.92	3.72	2.196	2.269	2.008
0	2.34	2.11	1.97	0.15	2.34	3.50	2.307	2.133	2.020

<sup>a</sup> See text for the parameters used in the calculations and definition of the electronic wave function.

$k_x = 0.79$ ,  $k_y = 0.84$ , and  $k_z = 0.70$  were used to account for the effects of covalency, with the excited-state energies being assumed to be similar to those in the pure copper(II) compound. The parameter  $\beta$  has been found to vary quite widely (from 50 to 500 cm<sup>-1</sup>) for different complexes, and the value deduced for the present system lies in the middle of this range.<sup>14</sup> The estimate of  $S_e$  is also quite similar to the values (55–200 cm<sup>-1</sup>) reported for the Cu(H<sub>2</sub>O)<sub>6</sub><sup>2+</sup> ion doped into various host lattices.<sup>10</sup> It may be noted that although the independent Cd—O bonds are crystallographically inequivalent in the triclinic phase, there is no significant difference in the bond lengths. However, a lattice strain similar to that deduced from the EPR of the copper complex would be expected<sup>10</sup> to cause a difference in bond lengths of only  $\sim 0.01$  Å in a Jahn–Teller inactive complex with similar bond force constants. Also, it must be remembered that the strain parameter is derived from the energy difference between the two orientations of the *distorted* complex (the geometries indicated by the filled and empty circles in Figure 2), so that an identical value is not to be expected or the host lattice.

The present model implies that the dramatic change in the g-tensor which accompanies the transition to the monoclinic phase of the host is due to the fact that the change in site symmetry causes the orthorhombic component of the strain to vanish (a small value of  $S_e$  must be retained in the calculations to represent the effects of random strains in the lattice).<sup>14</sup> The calculated g-values in the temperature range 300–370 K support this conclusion (Figure 5). Note that these calculations refer to the g-values along the bond directions; the slight anisotropy along the bisectors of these directions is explained in terms of a small rotation of the bond directions of the guest copper(II) complex with respect to those of the host (see preceding section).

Contour energy plots of the lower region of the Mexican hat potential surface for the copper(II) complex in the two phases of the host lattice are shown on the left side of Figure 6. The variation of the energy of this surface at a constant Jahn–Teller radius  $\rho = A_1/h\nu$  is shown on the right side of the figure (it should be noted that this does not represent the true path of lowest energy around the “trough” in the potential surface, since this is not precisely circular, as may be seen from the contour energy plots). The three wells in the potential surface are clearly seen, and it is evident that in overall terms the influence of the transition from the monoclinic to the triclinic phase of the host is quite modest, though the effect on the EPR spectrum is substantial.

The energies and composition of the wave functions calculated for the four lowest vibronic levels of the copper(II) complex in the two phases of the host lattice are shown in Table 5. Here, it must be recognized that the bond lengths estimated<sup>4,10</sup> from the vibrational components of the eigenfunctions

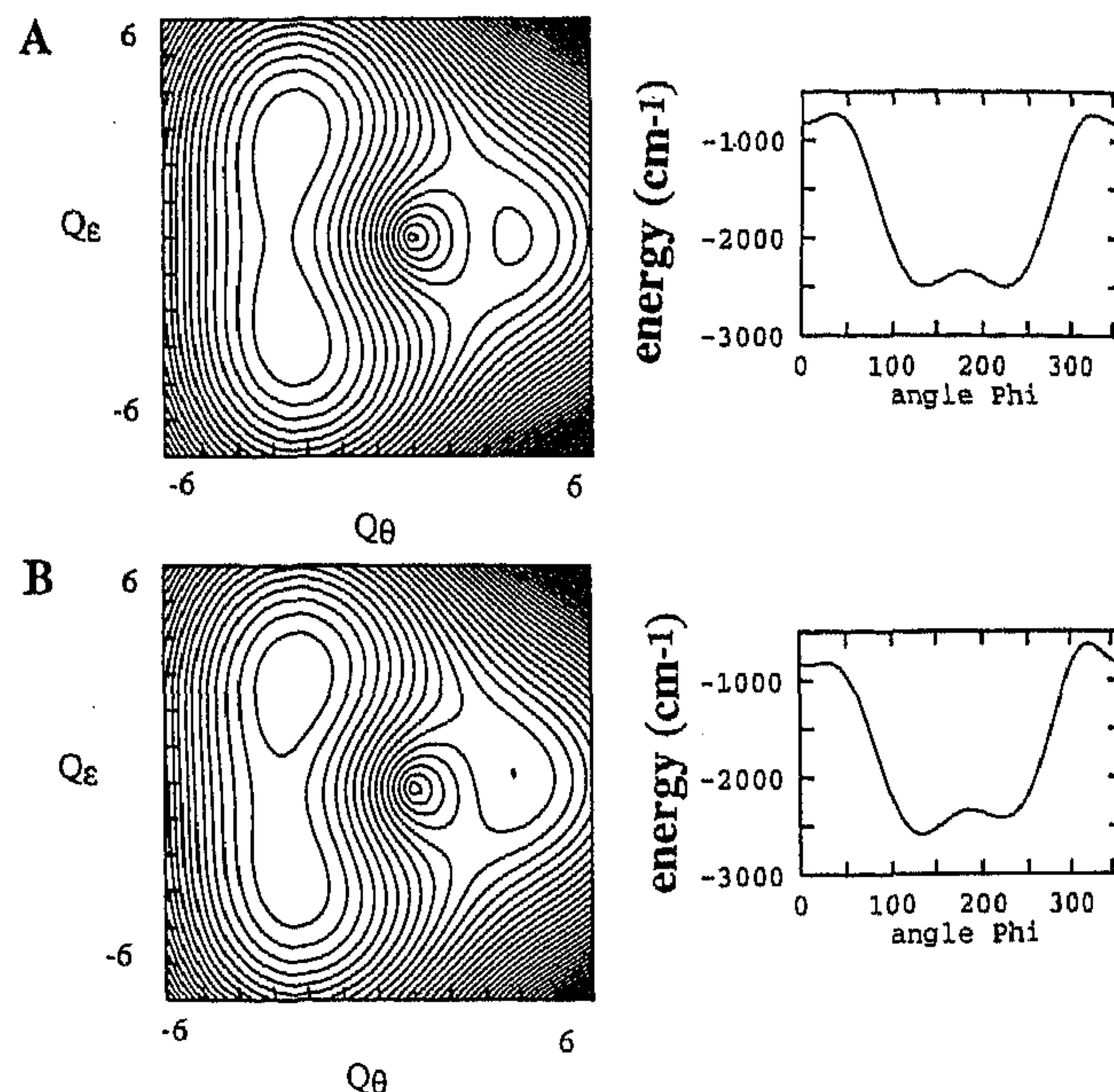


**Figure 6.** Contour energy plots of the lower region of the potential energy surface calculated for the copper(II) complex in Cu<sup>2+</sup>-doped (NH<sub>4</sub>)<sub>2</sub>[Cd(NH<sub>3</sub>)<sub>2</sub>(CrO<sub>4</sub>)<sub>2</sub>] for the high-temperature monoclinic (A) and low-temperature triclinic (B) phases of the host. The displacements in  $Q_\theta$  and  $Q_\epsilon$  are in dimensionless units as defined in ref 10. The contour energy interval is 125 cm<sup>-1</sup>. The variation of the energy minimum at a fixed Jahn–Teller radius of  $A_1/h\nu$  is shown on the right-hand side of each plot.

can only be expected to give a very approximate picture of the geometry associated with each level. This is largely because the extent to which interactions with the atoms outside the primary coordination sphere, in particular the other atoms of the chromate group, will influence the vibronic coupling is unknown. The basic geometry of the complex, calculated using an effective ligand mass of 16 amu and assuming an average bond length equal to that in the pure copper(II) complex, yields bond lengths for the lowest level in the triclinic cell of 1.97, 2.11, and 2.34 Å. These may be compared with the bond lengths of 1.97, 2.02, and 2.42 Å observed for the pure copper complex.<sup>8</sup> The electronic components of the wave functions, which are linear combinations of  $d_{x^2-y^2}$  and  $d_{z^2}$ , are conveniently expressed in the form<sup>18</sup>

$$\psi_e = cx^2 + ey^2 + fz^2$$

The expectation values of the squares of the coefficients  $c$ ,  $e$ , and  $f$  represent the probability that the unpaired electron will



be found along the *x*, *y*, and *z* Cartesian axis, and inspection of the values in Table 5 shows that, as expected, there is an inverse correlation between the magnitude of each coefficient and the bond length along that axis. The electronic component of the ground state of the complex in the triclinic phase of the host corresponds to an orbital which is predominantly  $d_{x^2-y^2}$  in character, with a modest admixture of  $d_{xz}$ . Note that the axis system is defined with *z* along the direction of the principal axis of the strain, the Cd–N bond direction.

The behavior of system exhibiting a temperature dependence of the *g*-values similar to that observed for the present triclinic system has generally been interpreted<sup>19</sup> using a model, originally proposed by Silver and Getz,<sup>9</sup> which involves just a single higher energy state having identical *g*-values to the ground state but with the higher two *g*-values reversed in direction. It was essentially this model which provided the qualitative picture presented in the previous section. The present results suggest that while this is basically correct, it probably provides an oversimplified picture of the nature of the upper state. As expected, along the Cu–N bond direction the wave function parameters, *g*-values and bond lengths are very similar for all four vibronic levels. However, although the relative magnitudes along the other two directions do interchange on going from the ground to the first vibronic level, the anisotropy decreases substantially. In fact, the first two upper levels, which are energetically quite close, both exhibit *g*-tensors in which the *g*-values along the Cu–O directions are quite similar. This reflects the fact that these wave-functions are quite delocalized over the two lower wells. Similar behavior has been noted for other systems<sup>10,20</sup> and is to be expected when the effects due to the orthorhombic component of the strain are comparable to those of the warping interaction represented here by  $\beta$ .

For the complex in the monoclinic, high-temperature phase of the host, the parameters in Table 5 suggest that, in general terms, the wave functions associated with the potential surface conform to the basic model in section 3.2.1. This suggests that a dynamic equilibrium occurs between two tetragonally elongated octahedral complexes which differ in the direction of the bonds and associated electronic wave function parameters along the Cu–O directions (*x* and *y*). The difference compared with the low-temperature phase is that here, because of the higher lattice symmetry, the two forms are energetically equivalent. However, here also, the calculations suggest that it may be too

simplistic to consider an equilibrium between two structural isomers with geometries similar to that of the pure copper(II) complex. This is because, if the orthorhombic component of the strain is strictly zero, the lowest vibronic states will be a pair of closely spaced energy levels each delocalized over the two potential energy minima. It was recognized by Ham<sup>21</sup> that in practice random imperfections will cause the minima to become slightly inequivalent at each lattice site. This acts to localize the wave functions in each well. In the present model, the effect of the random strains is included by the use of a nonzero value for  $S_e$ , and the parameters in Table 5 were obtained using  $S_e = 10 \text{ cm}^{-1}$ . This is somewhat higher than the value of  $S_e = 1.5 \text{ cm}^{-1}$  which was found to reproduce the low-temperature EPR spectrum of the Cu(H<sub>2</sub>O)<sub>2</sub>Cl<sub>4</sub><sup>2-</sup> center of Cu<sup>2+</sup>-doped NH<sub>4</sub>Cl.<sup>4</sup> The value of the strain necessary to localize the vibronic wave functions depends on the barrier height between the minima, and because this is thought to be rather high in the present compound (Figure 6) a relatively large value of the random strain is required to localize the vibronic wavefunctions. Because the *g*-values cannot be measured at low temperature for the monoclinic phase of Cu<sup>2+</sup>-doped (NH<sub>4</sub>)<sub>2</sub>[Cd(NH<sub>3</sub>)<sub>2</sub>(CrO<sub>4</sub>)<sub>2</sub>], the value of the random strain and extent of the localization cannot be determined experimentally. Within the framework of the present model, a value  $S_e = 15 \text{ cm}^{-1}$  would cause strong localization, with *g*-values similar to those of the lowest well of the potential surface of the triclinic phase, while a value  $S_e = 1.5 \text{ cm}^{-1}$  would leave the levels quite delocalized ( $g_1 = 2.221$ ,  $g_2 = 2.233$ ,  $g_3 = 2.013$  and  $g_1 = 2.201$ ,  $g_2 = 2.248$ ,  $g_3 = 2.018$ , for the two lowest levels, respectively). Thus, while the nature of the guest species in Cu<sup>2+</sup>-doped (NH<sub>4</sub>)<sub>2</sub>[Cd(NH<sub>3</sub>)<sub>2</sub>(CrO<sub>4</sub>)<sub>2</sub>] may be inferred in general terms, the details of the molecular geometries and ground-state wave functions of the species involved in the dynamic equilibria remain ambiguous.

**Acknowledgment.** Financial support from the Australian Research Council is acknowledged by M.A.H.

**Supporting Information Available:** Tables S1–S4, giving experimental details of the structural determinations, possible hydrogen bonds in CHOMH and CHROML(A), and thermal ellipsoid parameters (5 pages). Ordering information is given on any current masthead page.

IC950161H

(19) Hathaway, B. J. *Struct. Bonding* 1984, 57, 55.

(20) Beendorf, J.; Bürgi, H. B.; Gamp, E.; Hitchman, M. A.; Reinen, R.; Riley, M. J.; Stratemeier, H. Unpublished results.

(21) Ham, F. S. *Phys. Rev. A* 1965, 138, 1727; *Phys. Rev.* 1968, 166, 307.